DETERMINATION OF DYNAMIC DERIVATIVES OF RE-ENTRY VEHICLES USING UNSTEADY CFD SIMULATIONS.

Dominique Charbonnier, Jan B. Vos

CFS Engineering SA, EPFL Innovation Park A, 1015 Lausanne, Switzerland
dominique.charbonnier@cfse.ch, jan.vos@cfse.ch

ABSTRACT

The aerodynamic performance of large drag shapes like capsules or other spacecraft without wings is relatively poor during the atmospheric re-entry phase. This implies that it is necessary to investigate the dynamic behavior of these shapes to avoid an unstable behavior caused by small disturbances of the surrounding flow that can occur during this critical flight phase. Various strategies are commonly used to investigate the dynamic behavior, among them experimental measurements (wind tunnel or free flight tests) and numerical simulations. Both strategies can be combined to confirm the dynamic behavior obtained, or to validate the development of the numerical tools.

1. INTRODUCTION

For the investigations of the dynamic derivatives, two techniques are typically applied: forced oscillations or free oscillations. The forced oscillations technique is mostly used for aircrafts and winged bodies, especially since this technique is easier to implement in the case of experimental measurements. The free oscillations technique can be applied more easily in the context of numerical investigations, through the use of unsteady CFD simulations that include 6-DoF modeler and a moving grids capability. From a physical point of view, forced oscillations add energy to the flow field, that further excites the wake region, which is a critical region for the re-entry vehicles [1]. Indeed, the dynamic behavior of a re-entry body is mainly driven by the large recirculation near wake, or near the shoulder radius in the case of a capsule, where the viscous effects are predominant. With free oscillations, the inertia of the body removes energy from the flowfield, reducing the amplification of the wake response.

This paper presents the methodology to determine from unsteady CFD simulations the dynamic derivatives, and examples for different configurations are shown. Unsteady simulations have been performed using the NSMB (Navier Stokes Multi Block) CFD code, widely used for ESA funded projects in the field of atmospheric re-entry of space vehicles like capsules (ARD, ARV, EXPERT) or non-winged bodies (IXV, SpaceRider) [2]. For the purpose of describing properly the coupling between the body motion and the flow-field the ALE capability of the NSMB flow solver has been applied. Depending on the flow conditions, advanced turbulence models, like hybrid RANS-LES methods (DES/DDES turbulence modeling), have been also selected to ensure an accurate characterization of the flow physics, especially in the wake region.

In order to determine the dynamic damping derivatives from these unsteady CFD simulations, two data reduction methodologies have been implemented as post-processing tools and have been applied in recent research projects. The first methodology, that will be shown, allows for determining the mean value of the pitch damping coefficient, while the second methodology permits the extraction of the pitch damping coefficient with its dependency on the angle of attack. Results will be shown for the MarcoPolo ERC capsule, the SpaceRider lifting-body vehicle, as well as the Mars Entry Descent and Landing penetrator system.

Index Terms— Computational Fluid Dynamics, Dynamic Derivatives, Re-entry Vehicles

2. CFD SOLVER AND MESH GENERATION

2.1. The NSMB CFD solver

All the simulations reported in this paper were made using the NSMB "Navier Stokes Multi Block" CFD code. The NSMB code, described in [2,3,4] has a parallel and a vectorial structure and it can run on high-performance computers to solve a wide range of industrial aerodynamics design problems, and was mainly used for aeronautics and aerospace applications since more than 20 years.

NSMB solves the Reynolds-averaged Navier Stokes equations on multi-block structured grids. The code is compressible, using pre-conditioning or the artificial compressibility method for incompressible flows. NSMB offers all functionalities of a modern CFD code used for aerospace applications, ALE (Arbitrary Lagrangian Eulerian) approach, turbulence models, chemistry modeling, grid flexibility, FSI (Fluid-Structure Interactions) coupling,

Chimera overlapping technique, and has an extremely robust implementation of the LU-SGS time integration scheme. Several well tested and validated turbulence modeling approaches are implemented in NSMB (algebraic Baldwin-Lomax [5], one-equation Spalart-Allmaras [6], two-equation k-ω or k-ε [7, 8, 9],...) as well as more advanced models like LES and hybrid approaches known as DES/DDES for unsteady flows. Several variants of the Detached Eddy Simulation (DES) approach proposed by Spalart [10] are available in NSMB. In particular the variant from Dacles et al. [11] was selected for some cases due to its higher correction on the rotational production term for laminar vortex.

NSMB uses the ALE approach to simulate flows on moving grids. Three levels of ALE are distinguished:

- steady ALE - used to simulate flows on non-moving grids, as for example flows in a rotating frame.
- moving grids - used to simulate flows on moving grids, but no grid deformation takes place. This is typically used for calculations to determine dynamic derivatives
- deforming grids. This includes a re-meshing option using either the Volume Spline Interpolation or the Transfinite Interpolation technique. This is typically used for Fluid – Structure interactions simulations.

For the simulations of the dynamic stability of a capsule or vehicle the second type of ALE approach is employed since the simulations were performed considering the movement of the body grid relative to referential frame. In practice it means that the inviscid flux terms in the Navier Stokes equation are modified to include the flux due to the grid movement.

The 6DoF modeller computes the movement of the body after its release at initial conditions. The initial conditions are obtained from a steady state simulation at initial aerodynamic conditions, but without the motion of the grid during this phase. Then the 6DoF modeller combines the translation of the body in a 3-dimensional space with the rotation around the 3 axes under the effects of the gravity and the aerodynamic forces and moments.

To summarize the steps of the 6DoF modeller at each time step of the unsteady simulation, once the aerodynamic forces and moments are converged and known:

- compute the new body position (and its time derivatives) by resolving the translational dynamic equation
- compute the new body orientation (and its time derivatives) by resolving the rotational dynamic equation
- translate and rotate the computational grid following these new values using the ALE feature for moving grids available within NSMB.

2.2. Mesh generation

The ANSYS® ICEM CFD™ pre-processer tool was used to generate the multi-block structured grids needed by the NSMB flow solver. Since all the unsteady simulations are performed without restriction in the movement (6DoF motion), the grid topology was always generated for a full configuration.

To resolve the viscous boundary layer an O-grid topology with a geometric cell distribution was used around the whole bodies presented in the results section. The first cell height in the wall normal direction was set to obtain a $y+$ value close to/below 1 to ensure the proper use of low-Reynolds turbulence modeling, and the growth ratio of the cells normal to the wall was typically close to 1.2. Particular attention was paid to the refinement of the mesh close to the shoulder radius for the capsule shape, which can strongly affect the location of the separation point that occurs in this region, depending of the angle of attack. Detailed views of the different meshes are shown in Figure 1, Figure 2 and Figure 3.

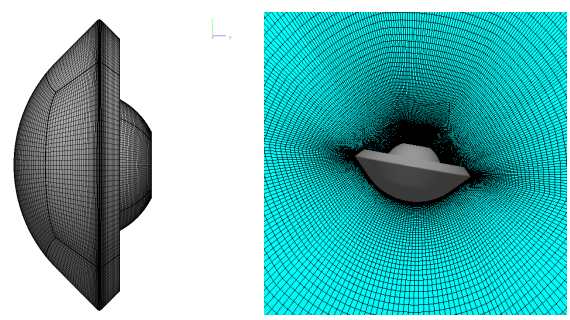

Figure 1: MarcoPolo ERC mesh (side view and symmetry plane view)

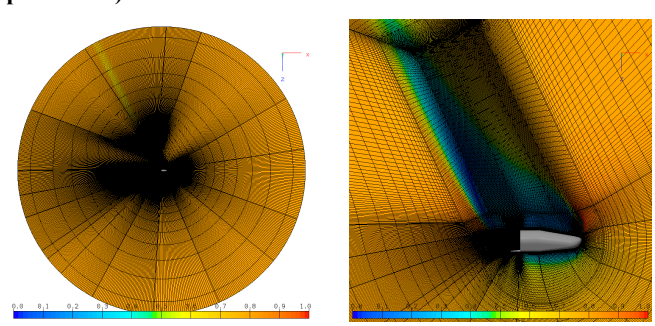

Figure 2: Structured grid in the symmetry plane for SpaceRider (farfield view and zoom view)

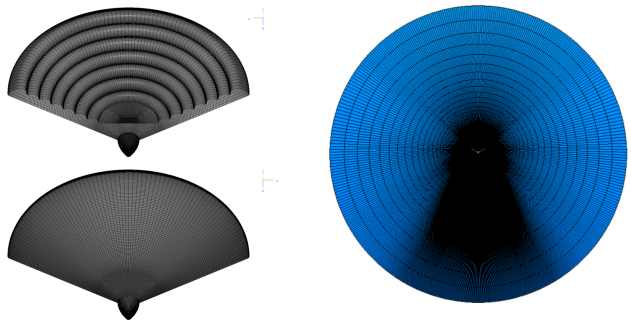

Figure 3: Mars Penetrator system mesh (on the leeward and windward surfaces, and in the symmetry plane)

For most of the computations, the far-field domain was designed as a sphere large enough to avoid pressure wave reflections at this boundary that might affect the computation of the aerodynamic coefficients. This has been investigated for different kind of bodies, and no particular influence was observed on the aerodynamic coefficients with the far-field distance at 10 times the maximum diameter of the capsule (or the length of the body), in comparison with a far-field distance at 25 times.

3. PITCH-DAMPING RECONSTRUCTION METHODOLOGIES

One of the key parameters to evaluate the dynamic stability of a body is the pitch-damping coefficient Cm_q, usually taken as the pitch-damping sum $Cm_q + Cm_{\dot{\alpha}}$, which indicates a damping behavior when its value is negative. From the time evolution of the attitude and the aerodynamic coefficients of the body obtained by the unsteady simulations, one can obtain this pitch-damping sum using the following procedures.

3.1. Pitch-damping sum – mean value

Considering the unsteady motion of the body in the symmetry plane, the equation of motion of the angle of attack α (which is equal to the pitch angle in the case of a movement with zero flight path angle) can be expressed as a 2nd order differential equation:

$$\ddot{\alpha} - \frac{\rho VS}{2m}\left(-CL_\alpha + \frac{mL^2}{2I}\left(Cm_q + Cm_{\dot{\alpha}}\right)\right)\dot{\alpha} - \frac{\rho V^2 SL}{2I} Cm_\alpha \alpha = 0$$

In this equation CL_α is the lift slope, Cm_α the pitching moment slope and $Cm_q + Cm_{\dot{\alpha}}$ the pitch-damping sum that corresponds to the relevant term to evaluate the dynamic stability of the body. The 2nd order differential equation above admits an explicit solution for the angle of attack as a function of time, which can be written as:

$$\alpha = Ae^{\xi t}\cos(\omega t + \delta)$$

where ξ stands for the damping factor, and ω for the angular frequency of the oscillator.

$$\xi = \frac{\rho VS}{4m}\left(-CL_\alpha + \frac{mL^2}{2I}\left(Cm_q + Cm_{\dot{\alpha}}\right)\right)$$

$$\omega = \sqrt{-\frac{\rho V^2 SL}{2I} Cm_\alpha}$$

The four unknowns A, ξ, ω and δ can be obtained using a non-linear curve fitting process applied to the angle of attack evolution curve obtained from the simulation (or experiment). Then the lift slope CL_α can be obtained by a linear regression of the lift coefficient curve as a function of the angle of attack, as well as the pitching moment slope Cm_α, which can be either derived directly from ω or obtained by a linear regression of the pitching moment curve as a function of the angle of attack.

Finally, when all these parameters are known the pitch-damping sum can be computed from:

$$\left(Cm_q + Cm_{\dot{\alpha}}\right) = \frac{2I}{mL^2}\left(\frac{4m}{\rho VS}\xi + CL_\alpha\right)$$

3.2. Pitch-damping sum - Angle of attack dependency

The post-processing of the pitch-damping sum Cm_q can also be done with another methodology in order to extract the angle of attack dependency of the coefficient. This second methodology is reported in [12] and partially in [1].

The method consists in:

- extract the points on the α curve (angle of attack α as function of time) for a given angle of attack α, as shown in Figure 4;
- introduce these points in a Cm diagram (pitching moment coefficient Cm as function of reduced pitch rate k_q) as reported in Figure 5;
- determine the slope by a linear regression to extract the Cm_q.

$$\left(Cm_q + Cm_{\dot{\alpha}}\right) = \frac{2V_\infty}{d}\frac{\partial C_m}{\partial q} = \frac{\partial C_m}{\partial k_q}$$

with k_q the reduced pitch rate expressed by:

$$k_q = \frac{qd}{2V_\infty}$$

with q the pitch rate and d the diameter (L_{ref}).

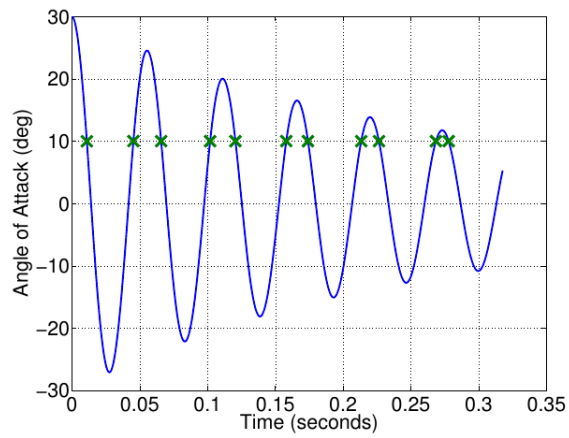

Figure 4: Time-evolution of the angle of attack [12]

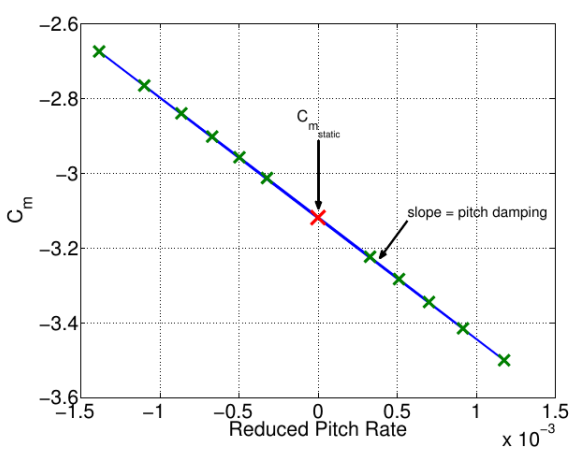

Figure 5: Pitching moment coefficient as function of reduced pitch rate [12]

4. RESULTS OF CALCULATIONS

The methodologies described in the sections 3.1. and 3.2. have been applied on re-entry vehicles in the last few years. The first method "mean value" was mainly applied during the dynamic stability analysis for the MarcoPolo-R capsule [13] and the SpaceRider lifting-body vehicle, while the second method "AoA dependency" was implemented and applied for the Mars Penetrator Entry Descent and Landing (EDL) system analysis.

4.1. MarcoPolo-R capsule

One of the objectives of the ESA study on the MarcoPolo-R capsule was to apply the most relevant CFD methods to compute the dynamic stability derivatives. The shape of the capsule is shown in Figure 1.

Five unsteady simulations have been performed with the main objective to populate the AEDB in subsonic regime between the experimental VMK results (vertical wind tunnel at DLR in Koln) and the ISL results (ballistic flight). The computational parameters as well as the results obtained for the dynamic coefficients using the reconstruction process described in section 3.1. are given in Table 1.

purpose	**extrapolation to flight**			**flight prediction**	
scale [m]	full scale 0.88				
Mach	0.6	0.2	0.2	0.7	0.95
XoG [%L]	30	30	25	25	25
AoA$_0$	10º				
turb. model	DDES Spalart-Allmaras				
cycles	5	5	5	3.5	5
$\boldsymbol{CL_\alpha}$	0.375	0.375	0.385	0.416	0.651
$\boldsymbol{Cm_\alpha}$	-0.143	-0.150	-0.179	-0.172	-0.155
$\boldsymbol{Cm_q}$	-0.018	-0.095	-0.103	-0.056	-0.219

Table 1: Dynamic computational campaign parameters and dynamic coefficients results

Typical curves of pitch angle, aerodynamic coefficients, position time history as well as fitting curves of the pitching moment and lift coefficients for the case at Mach 0.6 are shown in Figure 6. The non-linear fitting curve of the pitch angle can be seen in the top/left picture, and the value of ξ shown in this picture corresponds to the damping factor parameter that allows computing the pitch damping sum. One can note that the curve fitting has been started after the first cycle in order to avoid discrepancies due to the initialization phase of the computation. The negative value of the pitch damping sum Cm_q indicates the damped behavior of the capsule at the selected flight parameters.

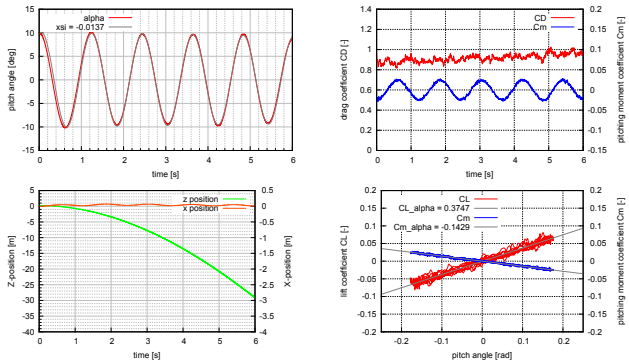

Figure 6: Time history of pitch angle, drag and pitching moment coefficients, relative position – pitching moment and lift fitting curves – MarcoPolo-R capsule

4.2. SpaceRider lifting-body vehicle

In the SpaceRider project (phase A), dynamic derivatives of the vehicle have been assessed by means of forced oscillations (plunging motion and pitching motion) technique and free oscillations technique. Only the results obtained with the free oscillations technique is discussed in this paper. Figure 7 gives an overview of the computational domain and the flow field around the SpaceRider body, which has a similar shape as the IXV vehicle (Intermediate eXperimental Vehicle). During the free oscillations computations campaign, 4 time-steps were tested, 0.1s, 0.05s, 0.01s and 0.001s. Time history of the pitch angle variation (Figure 8) shows that the smallest time-step 0.001s gives a very similar trend on the 2 first periods in comparison with the time-step 0.01s. Then the result of the computation with time-step 0.01s is considered as converged in time.

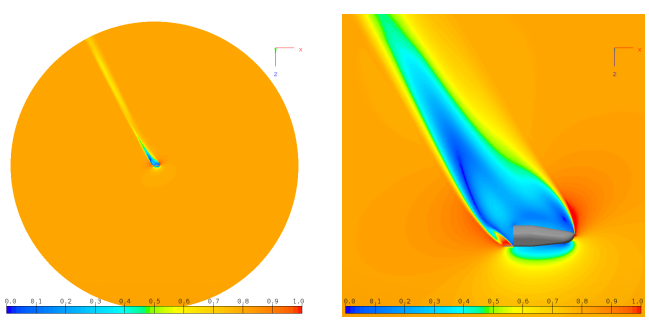

Figure 7: Mach number distribution in the symmetry plane (full domain on left, zoom on the IXV vehicle on right)

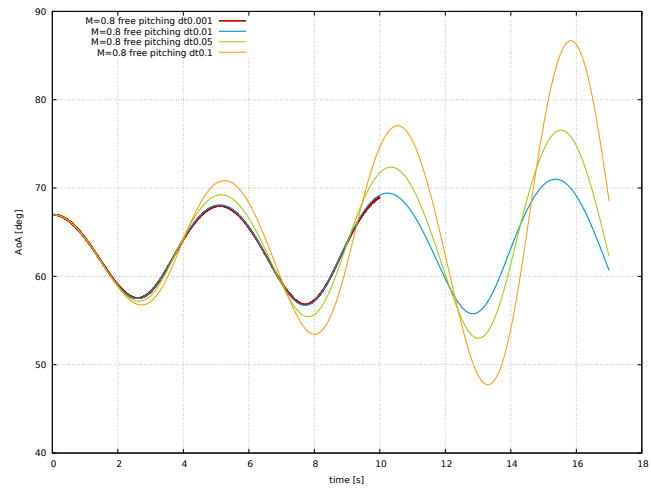

Figure 8: Time history of pitch angle for different values of time-step – SpaceRider free pitching oscillations computation

Figure 9 and Figure 10 show the curve fitting process described in section 3.1. for dynamic coefficient Cm_q reconstruction and summarizes the values of the damping factor, lift slope coefficient and pitching moment slope coefficient for the simulation with a time-step of 0.01s. Based on these values, the mean pitch damping sum was derived and reported in Table 2. The result of the fitting process indicates a diverging behavior, which has been also observed in the comparison with coefficients estimated by Dassault based on the AEDB results [14]. However, a strong effect of computing time step has been identified with the estimation of Cm_q obtained with other time-steps (not reported in this paper): decreasing time step decreases divergence, reaching a neutral behavior.

		α=A.exp(ξt).cos(ωt+δ)				CL(α)=CLα.α		Cm(α)=Cmα.α
case	**time-step**	**ξ**	**A**	**ω**	**δ**	**Cmq+Cmadot**	**CLα (fit)**	**Cmα (from ω)**	**Cmα (fit)**
M0.8_free_pitching_dt0.01	0.01	**0.0340**	-4.6640	1.2235	-3.1037	**0.556**	**-1.059**	**-0.214**	**-0.211**

Table 2: Pitch damping coefficient evaluation for free pitching oscillations

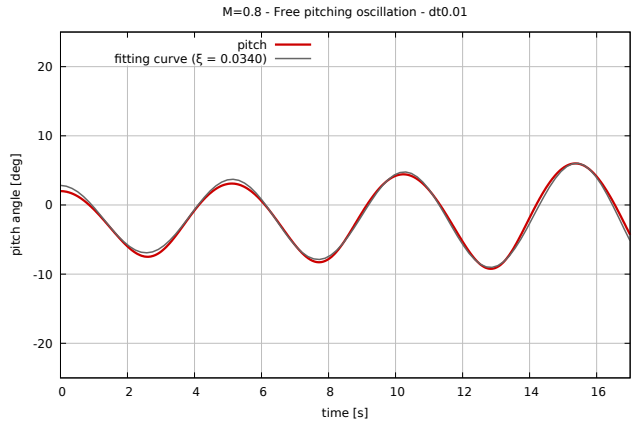

Figure 9: Curve fitting of the pitch angle with extracted value of the damping factor ξ – SpaceRider free pitching oscillations computation

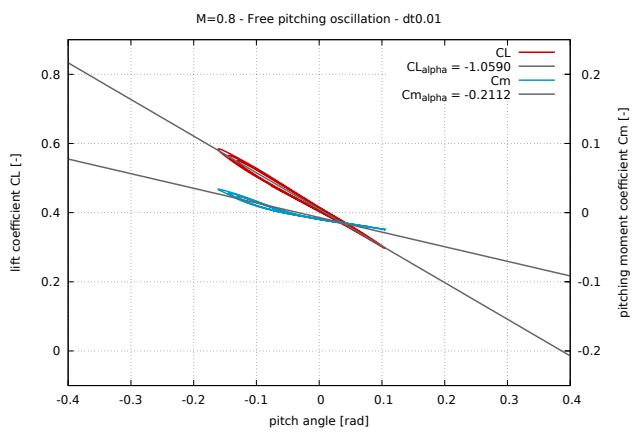

Figure 10: Curves fitting with extracted values of lift slope CL_α and pitching moment slope Cm_α – SpaceRider free pitching oscillations computation

4.3. Mars EDL Penetrator system

Estimation of the dynamic derivatives was part of the "Mars Penetrator - Entry Descent and Landing system" project, for which a large number of CFD simulations were made [15]. The original shape of the Penetrator system is given in Figure 3. The dynamic movement of the system, with an amplification of the pitch oscillations around the center of gravity, shows an instability of the system at the subsonic flow regime with this original shape. Since the steady simulation at that flow regime also show an unstable wake behind the body, it was decided to investigate the effect of the afterbody shape of the penetrator system on the dynamic behavior. The penetrator system was closed behind the inflatable part by means of a flat shape (blue) or a round shape (green) as shown in Figure 11.

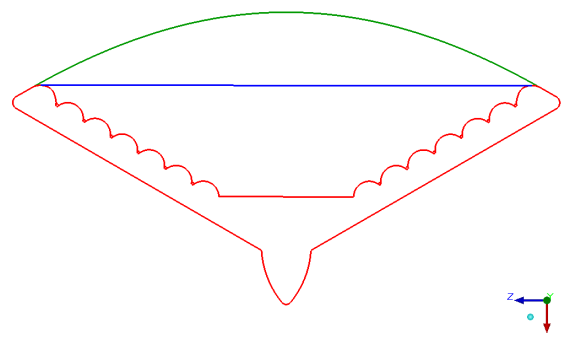

Figure 11: Modifications of the Penetrator system shape (leeward side)

The first methodology - mean value of Cm_q - has been applied to the unsteady computations and the results are reported in Table 3 for the three shapes of the penetrator system investigated.

case	time-step	ξ	A	ω	δ	$Cm_q + Cm_\dot{\alpha}$	CL_α (fit)	Cm_α (from ω)	Cm_α (fit)
original	0.001	0.1191	22.9556	2.1760	-18.2747	1.325	-0.900	-0.163	-0.162
closed flat	0.001	0.0973	15.0294	2.2841	-18.2180	1.056	-0.915	-0.179	-0.177
closed round	0.001	0.0557	-17.1273	2.2720	-27.6100	0.537	-0.975	-0.177	-0.175
closed round	0.00025	0.0556	14.9788	2.3137	0.4248	0.534	-0.981	-0.184	-0.182

Table 3: Pitch damping coefficient evaluation – Penetrator system

The fitting curves that permit to obtain the various unknown factors A, ξ, ω and δ as well as the slopes CL_α and Cm_α are presented in Figure 12 and Figure 13 for the round shape closure case computed on the penetrator system. The grey areas on the graphs with time evolution of the angle of pitch correspond to part of the curves that are not taken into account for the curves fitting process. These areas are excluded to remove the sensitivity of the computation at the start where there is a transition between the steady and the unsteady simulations and at the end where the angle of the model becomes too high.

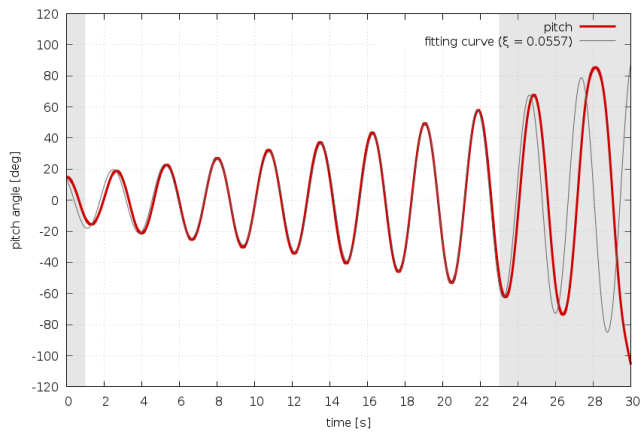

Figure 12: Curve fitting for damping factor ξ estimation - Penetrator system with round shape closure (dt=0.001s)

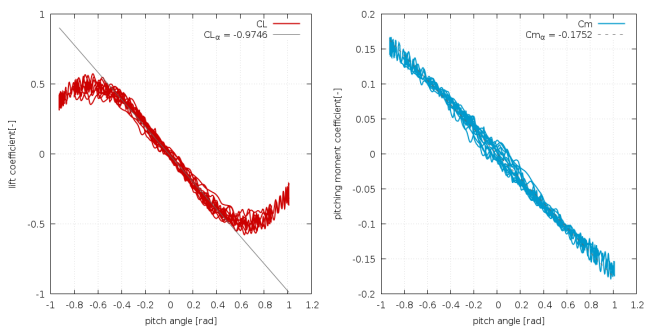

Figure 13: Curves fitting for slopes CL_α and Cm_α estimation - Penetrator system with round shape closure (dt=0.001s)

One can observe that the penetrator system has an undamped behavior for the round closure shape reported in Figure 12 (but also for the two other shapes not reported in this paper), with positive values for Cm_q. However, as expected, the shape with flat or round closure of the leeward side of the system shows a significant reduction of the amplitude of the pitch oscillations with an increase of the number of oscillations periods. During the project a small sensitivity to the time step was observed, and time-steps of 0.001s and 0.00025s were tested. It was found that the amplitude of the oscillations is slightly reduced with the smaller time-step but the value of the Cm_q remains very close (see also Table 3).

The second methodology to extract the Cm_q with angle of attack dependency has been applied firstly on the three cases (original, closed flat and closed round) for the penetrator system. The comparison of the two methods is shown in Figure 14. The solid lines represent the Cm_q as function of angle of attack. Cmq_{avg} reports the average value of the Cm_q obtained by the second methodology (averaged value of the solid line) while Cmq_{mean} reports the mean value of Cm_q obtained by the first methodology. One can observe that the results are coherent, with close values between Cmq_{avg} and Cmq_{mean} for the three different configurations. However, one can note a significant sensitivity of both methods to the extraction parameters (number of oscillations, range of the angle of attack, time range selected for the fitting, ...).

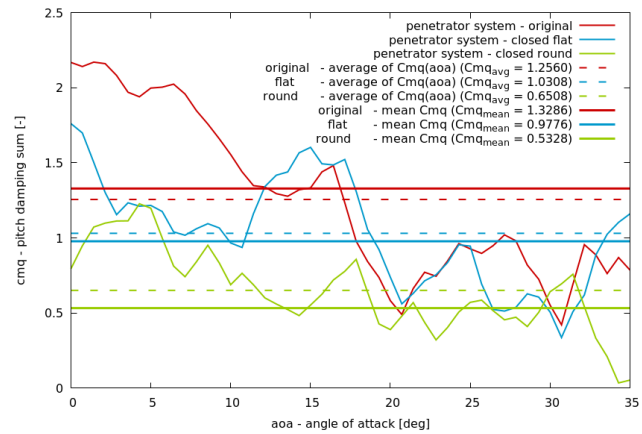

Figure 14: Pitch-damping sum - Comparison of the two extraction methods

Finally, the effect of turbulence modeling has been evaluated. The configuration with the penetrator system closed with the round shape has been computed including turbulence modeling. The computation parameters were exactly the same as for the laminar case. The hybrid DDES approach proposed by Spalart has been chosen for turbulence modeling like during the MarcoPolo project. The Spalart-Allmaras model available in the NSMB code (Dacles variant [11]) has been selected due to its higher correction on the rotational production term for laminar vortex. The results of this additional turbulent computation are reported in Figure 15 and compared to the laminar case. The results show a slight decrease (around 7% with both methods) of the pitch-damping sum obtained with the turbulence modeling. However, the pitch-damping sum remains always positive.

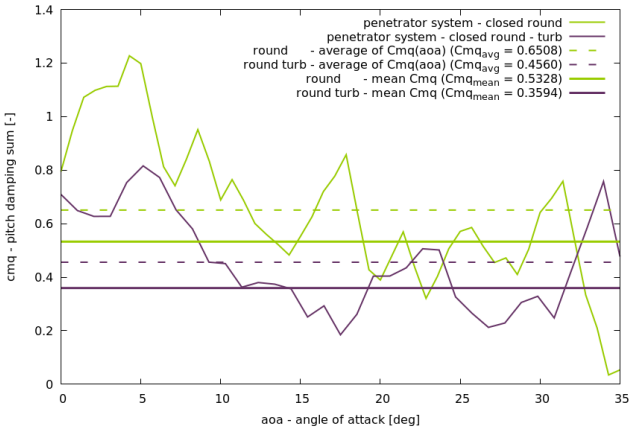

Figure 15: Pitch-damping sum - Comparison of laminar and turbulent cases

5. CONCLUSION

The dynamic damping derivatives can be evaluated using unsteady CFD simulations and dynamic coefficients extraction methods. Two Cm_q reconstruction methodologies have been implemented as post-processing tools (written in Python and using included mathematical and statistical libraries) and have been applied in recent research projects. The first methodology, used since few years, allows for determining the mean value of the pitch damping sum, while the second methodology, used more recently, extracts the pitch damping sum with its dependency to the angle of attack.

Results of these reconstruction methodologies applied on different re-entry vehicles show that the presented methods are able to extract the pitch damping sum from unsteady simulations, coherent with results from other determination techniques (experimental or numerical). The mean values of Cm_q obtained with both methods are also close, which gives a good confidence. However, attention needs to be paid to the sensitivity of the methods to the extraction parameters (number of oscillations, time range, angle of attack range…).

6. REFERENCES

[1] S.M. Murman and M.J. Aftosmis, "Dynamic Analysis of Atmospheric-Entry Probes and Capsules", 45th AIAA Aerospace Sciences Meeting, Reno, NV, AIAA 2007-0074, January 8-11 2007

[2] J.B. Vos, A.W. Rizzi, A. Corjon, E. Chaput and E. Soinne, "Recent Advances in Aerodynamics inside the NSMB (Navier Stokes Multi Block) Consortium", Invited Talk AIAA 36th Aerospace Sciences Meeting, January 1998.

[3] J.B. Vos, A.W. Rizzi, D. Darracq, and E.H. Hirschel, "Computational Aerodynamics for Industrial Airframe Design using Navier Stokes Solvers", Progress in Aerospace Sciences, Vol. 38, pp. 601-697, 2002.

[4] Y. Hoarau, D. Pena, J.B. Vos, D. Charbonnier, A. Gehri, M. Braza, T. Deloze, E. Laurendeau, "Recent Developments of the Navier Stokes Multi Block (NSMB) CFD solver". AIAA Scitech Conference, 2016-2056.

[5] B.S. Baldwin and H. Lomax, "Thin Layer Approximation and Algebraic Model for Separated Turbulent Flows", AIAA-paper 78-257, 1978.

[6] P.R. Spalart and S.R. Allmaras, "A One-Equation Turbulence Model for Aerodynamic Flows", AIAA Paper 92-0439, Jan. 1992.

[7] D.C. Wilcox, "Turbulence Modeling for CFD", DCW Industries, Inc. La Casada, California, 1993.

[8] F.R. Menter, "A Zonal Two Equation k-w Turbulence Models for Aerodynamic Flows", AIAA paper, vol. 93-2906, 1993.

[9] R. Langtry and F.R. Menter, "Correlation-based transition modeling for unstructured parallelized computational fluid dynamic codes", AIAA Journal, Vol. 47, pp. 2894-2907, 2009.

[10] P.R. Spalart, "Detached Eddy Simulation", *Annual Review of Fluid Mechanics*, Vol. 41, pp. 181-202, 2009.

[11] J. Dacles-Mariani, D. Kwak, and G.G. Zilliac, "On Numerical Errors and Turbulence Modeling in Tip Vortex Flow Prediction", Int. J. for Numerical Methods in Fluids, Vol. 30, pp. 65-82, 1999.

[12] M.E. Bartowitz, "Determination of Static and Dynamic Stability Coefficients Using Beggar", Thesis, Air Force Institute of Technology, Ohio, 2008

[13] D. Charbonnier, J. B. Vos, E. Clopeau, L. Ferracina, L. Marraffa, "Marcopolo-R ERC Dynamic Characterization: Computational Campaign", ESA 8th Aerothermodynamics Conference, March 2015.

[14] Dassault Aviation internal document, "CFD computations for dynamic derivatives assessment", June 2017

[15] D. Chaillot, H.U. Quaranta, A. Santerre, G. Pinaud, J. Vos, L. Ferracina, "Aerothermodynamics assessment of an entry descent and landing system for a penetrator mission on Mars", FAR2019, 2019.